Vessel tortuousity and reduced vascularization in the fetoplacental arterial tree after maternal exposure to polycyclic aromatic hydrocarbons

Monique Y. Rennie, Jacqui Detmar, Kathie J. Whiteley, Jian Yang, Andrea Jurisicova, S. Lee Adamson and John G. Sled

Am J Physiol Heart Circ Physiol 300:H675-H684, 2011. First published 10 December 2010; doi:10.1152/ajpheart.00510.2010

Am J Physiol Heart Circ Physiol 300: H675–H684, 2011.
First published December 10, 2010; doi:10.1152/ajpheart.00510.2010.

Vessel tortuousity and reduced vascularization in the fetoplacental arterial tree after maternal exposure to polycyclic aromatic hydrocarbons

Monique Y. Rennie,[1,2,3] Jacqui Detmar,[3,4,6] Kathie J. Whiteley,[6] Jian Yang,[1] Andrea Jurisicova,[3,5,6] S. Lee Adamson,[3,5,6]* and John G. Sled[1,2]*

[1]*Mouse Imaging Centre, Hospital for Sick Children, Toronto, Ontario;* [2]*Department of Medical Biophysics,* [3]*Department of Obstetrics and Gynecology,* [4]*Institute of Medical Studies and* [5]*Department of Physiology, University of Toronto, Toronto, Ontario; and* [6]*Samuel Lunenfeld Research Institute, Mount Sinai Hospital, Toronto, Ontario, Canada*

Submitted 27 May 2010; accepted in final form 3 December 2010

Rennie MY, Detmar J, Whiteley KJ, Yang J, Jurisicova A, Adamson SL, Sled JG. Vessel tortuousity and reduced vascularization in the fetoplacental arterial tree after maternal exposure to polycyclic aromatic hydrocarbons. *Am J Physiol Heart Circ Physiol* 300: H675–H684, 2011. First published December 10, 2010; doi:10.1152/ajpheart.00510.2010.—Polycyclic aromatic hydrocarbons (PAHs) are ubiquitous environmental pollutants and the main toxicants found in cigarettes. Women are often exposed to PAHs before pregnancy, typically via prepregnancy smoking. To determine how prepregnancy exposure affects the fetoplacental vasculature of the placenta, we exposed female mice to PAHs before conception, perfused the fetoplacental arterial trees with X-ray contrast agent, and imaged the vasculature ex vivo by microcomputed tomography (micro-CT) at *embryonic day 15.5*. Automated vascular segmentation and flow calculations revealed that in control trees, <40 chorionic plate vessels (diameter >180 μm) gave rise to ~1,300 intraplacental arteries (50–180 μm), predicting an arterial vascular resistance of 0.37 ± 0.04 mmHg·s·μl^{-1}. PAH exposure increased vessel curvature of chorionic plate vessels and significantly increased the tortuousity ratio of the tree. Intraplacental arteries were reduced by 17%, primarily due to a 27% decrease in the number of arteriole-sized (50–100 μm) vessels. There were no changes in the number of chorionic vessels, the depth or span of the tree, the diameter scaling coefficient, or the segment length-to-diameter ratio. PAH exposure resulted in a tree with a similar size and dichotomous branching structure, but one that was comparatively sparse so that arterial vascular resistance was increased by 30%. Assuming the same pressure gradient, blood flow would be 19% lower. Low flow may contribute to the 23% reduction observed in fetal weight. New insights into the specific effects of PAH exposure on a developing arterial tree were achieved using micro-CT imaging and automated vascular segmentation analysis.

fetoplacental vasculature; polycyclic aromatic hydrocarbons; microcomputed tomography; prepregnancy smoking; placenta; smoking; mouse; pregnancy

POLYCYCLIC AROMATIC HYDROCARBONS (PAHs) are ubiquitous environmental pollutants and the main toxicants found in cigarettes (17). Both maternal smoking (5) and PAH exposure due to environmental air pollution (43) are associated with reduced fetal growth and various other morbidities (9, 48) in human pregnancy. Fetoplacental vascular resistance appears to be chronically elevated by smoking (1, 21, 36), and this would be anticipated to reduce fetoplacental blood flow thereby contributing to fetal growth restriction. A sustained increase in resistance suggests that smoking causes abnormalities in the growth and/or branching of the fetoplacental vascular tree. Consistent with this, smoking is associated with decreases in fetoplacental capillary surface area, volume, and length in human placentas (8, 25). Comparatively, there is a paucity of information on fetoplacental vascular insults in cases of prepregnancy PAH exposure and/or smoking.

The proportion of women who smoke during pregnancy has significantly decreased since the early 1990s (11, 29). Indeed, over the last decade, 26–47% of smoking women stopped smoking during pregnancy (51). However, PAHs can accumulate in adipose and mammary tissue before smoking cessation (33) and can be released into the blood stream during pregnancy (33). More than a year after smoking cessation, PAH-DNA adducts in human blood samples are reduced by only 50% compared with levels during smoking (34). PAHs have also been shown to accumulate in the placentas of non and ex-smokers in heavily polluted areas (16). Nevertheless, there is limited information on the effects of PAH accumulation on pregnancy outcomes.

In mouse models, prepregnancy exposure to PAHs (14) or environmental air pollutants (55) results in an apparent increase in fetoplacental capillaries that contrasts with decreased capillarization in the placentas of smoking mothers (8, 25). Nevertheless, fetal growth restriction is observed as a consequence of exposure whether before or during pregnancy. Capillaries are not generally considered to be a site of major vascular resistance to blood flow in the circulation. In the context of vascular resistance and its control, arterioles in particular are considered paramount. Thus, prepregnancy smoking and/or PAH exposure may cause defects in larger vessels, thereby contributing to increased fetoplacental vascular resistance and resulting in reduced fetal growth. Indeed, exposure to PAHs before pregnancy in mice reduced the volume and surface area of the fetoplacental arterial tree (vessels >30 μm), whereas veins appeared unaffected (14). Thus, as observed in smoking mothers (1, 21, 36), fetoplacental vascular resistance may be elevated, and this would be anticipated to reduce fetoplacental blood flow thereby contributing to fetal growth restriction.

The determinants of the branching pattern of the larger vessels of the arterial vascular tree are surprisingly poorly understood but likely depend on genetic, hemodynamic, and environmental factors. Our poor understanding related to formation of the placental vascular tree contrasts with a wealth of knowledge related to the initial specification, differentiation, and development of the nascent vasculature in the embryo (12) and control of branching morphogenesis of other structures such as the bronchi (35) and renal tubules (7). One of the

* S. L. Adamson and J. G. Sled were coprincipal investigators on this work.
Address for reprint requests and other correspondence: J. G. Sled, Mouse Imaging Centre, Toronto Centre for Phenogenomics, 25 Orde St., Toronto, ON, Canada M5T 3H7 (e-mail: jgsled@phenogenomics.ca).

challenges of assessing microvasculature morphology is the difficulty in obtaining accurate geometric data in a form that can be related to hemodynamic parameters. Recent advances in microcomputed tomography (micro-CT) imaging and computer analysis techniques have addressed this need and provide the automation needed to examine large numbers of specimens. A recent report demonstrated significant differences between the arterial branching patterns of the mouse fetal placenta and adult lung (59). Prior work on small numbers of specimens examined other organs, including the kidney (40), liver (41), and coronary vasculature (26).

The goal of the current study was to exploit advances in micro-CT imaging and computer analysis to quantify the branching pattern of the fetoplacental arterial tree of the mouse and to quantify the effect of prepregnancy PAH exposure on this vasculature. We subsequently used these data to predict the influence of such changes on fetoplacental vascular resistance.

MATERIALS AND METHODS

Mice. Experimental procedures were approved by the Animal Care Committee of Mount Sinai Hospital and conducted in accordance with guidelines established by the Canadian Council on Animal Care. Two groups of C57Bl6 virgin female mice (National Cancer Institute, Frederick, MD) were group-housed in separate cages. Subcutaneous injections of vehicle (corn oil) or PAHs were administered to the vehicle control and PAH-treated groups, respectively, over a 9-wk period as previously described (14). The cumulative dose over the 9-wk period for PAH-treated mice was 12 mg/kg, a dosage equivalent to ~7 cigarettes/day for 9 wk in humans. Vehicle-treated animals were given proportional injections of corn oil, according to body weight.

Females were mated to a male of proven fertility 4–5 days after the last injection. The morning that a vaginal copulation plug was detected was designated *embryonic day* (E) *0.5*. No injections were given during pregnancy. Pregnant mice were killed by cervical dislocation at E15.5, and their uteri were quickly removed and immersed in ice-cold PBS. At this stage, fetuses are growing rapidly, organogenesis is complete, and the placenta is near maximal in size (24).

Injection of contrast agent and CT scanning. A radio-opaque silicone rubber X-ray contrast agent (Microfil; Flow Tech, Carver, MA) was infused into the fetoplacental vasculature as previously described (47, 58). In brief, individual implantation sites were removed from the chilled uteri and weighed. The embryo and placenta were then surgically exposed and bathed in warm PBS to resuscitate the embryo and resume circulatory function. A double-lumen glass cannula (58) was advanced into the umbilical artery with the umbilical vein nicked to serve as a vent. Blood was cleared from the vasculature using heparinized saline with xylocaine as a vasodilator (58). The contrast agent was infused into the arterial vasculature until its bright yellow color could be seen in the capillary bed. At this point, the vessels were tied off to maintain pressure. The silicone rubber was allotted time to polymerize before the umbilical cord was severed, placental and embryonic weights were recorded, and the placenta was immersed in fixative (10% buffered formalin phosphate) for 24–48 h at 4°C. Specimens were mounted in 1% agar made with 10% formalin in preparation for ex vivo scanning. Specimens were obtained for vehicle controls ($n = 10$ from 4 litters) and PAH-treated mice ($n = 10$ from 5 litters), with a range of one to four specimens obtained from each dam in the study.

Three-dimensional (3D) datasets were acquired for each specimen using an MS-9 micro-CT scanner (GE Medical Systems, London, ON, Canada) as previously described (47). Each specimen was rotated 360° around the vertical axis, generating 720 views in 2 h. Subsequent reconstruction yielded 3D data blocks containing 500 × 500 × 500 13 μm voxel elements. Vascular surface renderings such as in Fig. 1*A* were generated from micro-CT data to visualize the arterial vasculature as we have described previously (47). Umbilical artery diameters and the span and depth of the fetoplacental arterial tree were measured directly from these surface renderings via digital calipers using the Amira software package (Visage Imaging, San Diego, CA). Prior work showed that umbilical artery diameters measured using this method were in close agreement with in vivo measurements obtained using microultrasound (47).

Automated vascular segmentation. Segmenting micro-CT datasets to identify blood vessels based on image intensity simplifies these large datasets into a form that is more meaningful and easily analyzed. Each dataset underwent a vascular segmentation process based on the algorithm of Fridman et al. (15) to automatically identify vessel-like structures in the image. Details of the segmentation algorithm can be found in the Supplemental Methods (Supplemental data for this article may be found on the *American Journal of Physiology: Heart and Circulatory Physiology* website.). In brief, this segmentation algorithm is based on finding the center lines of branching tubular objects in 3D grayscale datasets and extracting both the tubes themselves and their connectivity. The algorithm returns the center lines of a connected vessel tree, after which additional seeds (i.e., new starting points for the algorithm) can be manually placed in any vessels that were missed and the algorithm rerun (Fig. 1*B*). This process was repeated until all vessels were accounted for upon visual assessment, after which all newly added trees were extrapolated back to the main tree for connections, generating a tubular model for which the lengths, diameters, and connectivity of each vessel segment are known. Measurements of vessel segment numbers, diameter distributions, and distance to terminal vessels were extracted from the resultant tubular models (Fig. 1*C*).

During vascular segmentation, most premature terminations of the algorithm occurred when a small vessel branched off from a much larger vessel. In the placenta, this often occurs when small-diameter intraplacental arteries branch directly off the largest arteries of the chorionic plate. For example, in three arbitrarily selected datasets, a single root seed tracked ~1,000 vessels, which corresponded to >80% of the total number tracked and the total arterial volume. Additional passes to track all visible vessels resulted in datasets that accounted for >97% of the tree's volume. On average, datasets required 17 manually placed seeds (range: 7–44) applied during up to five additional segmentation passes.

Evaluation of segmentation method. Vessel diameters estimated by the algorithm are shown in Fig. 1*D*. To evaluate the diameter accuracy of the segmentation algorithm, a distribution of manually selected segment diameters generated by the segmentation program was compared with manual digital caliper measurements made on CT isosurface renderings such as that shown in Fig. 1*A*. Segments used in the evaluation were selected from four E15.5 and six E17.5 C57Bl6 placental datasets. Microfil-perfused segments of polyethylene tubing (Intramedic; Becton-Dickinson, Sparks, MD) with manufacturer-specified internal diameters of 0.279, 0.381, 0.584, and 0.760 mm were also added to this analysis. All isointensity surface reconstructions and digital caliper measurements used to assess accuracy were made using Amira visualization software. In total, 84 diameter measurements spanning a diameter range of 0.050–0.756 mm were compared. No significant difference was seen between manual and segmentation-generated measurements ($P = 0.274$). The average percent difference (Fig. 1*E*) was −2.89%, with measurements generated via segmentation tending to be smaller than their manual counterparts.

Measurement variability introduced by the micro-CT and vascular segmentation method was assessed by performing four repeated scans, reconstructions, segmentations, and analysis of the number of tracked segments recorded over the range of diameters for one control specimen. Cumulative distribution curves exhibited an inflection point at ~50 μm below which the slopes of the curves were noticeably decreased (Fig. 1*F*). This suggests that vessels smaller than this were

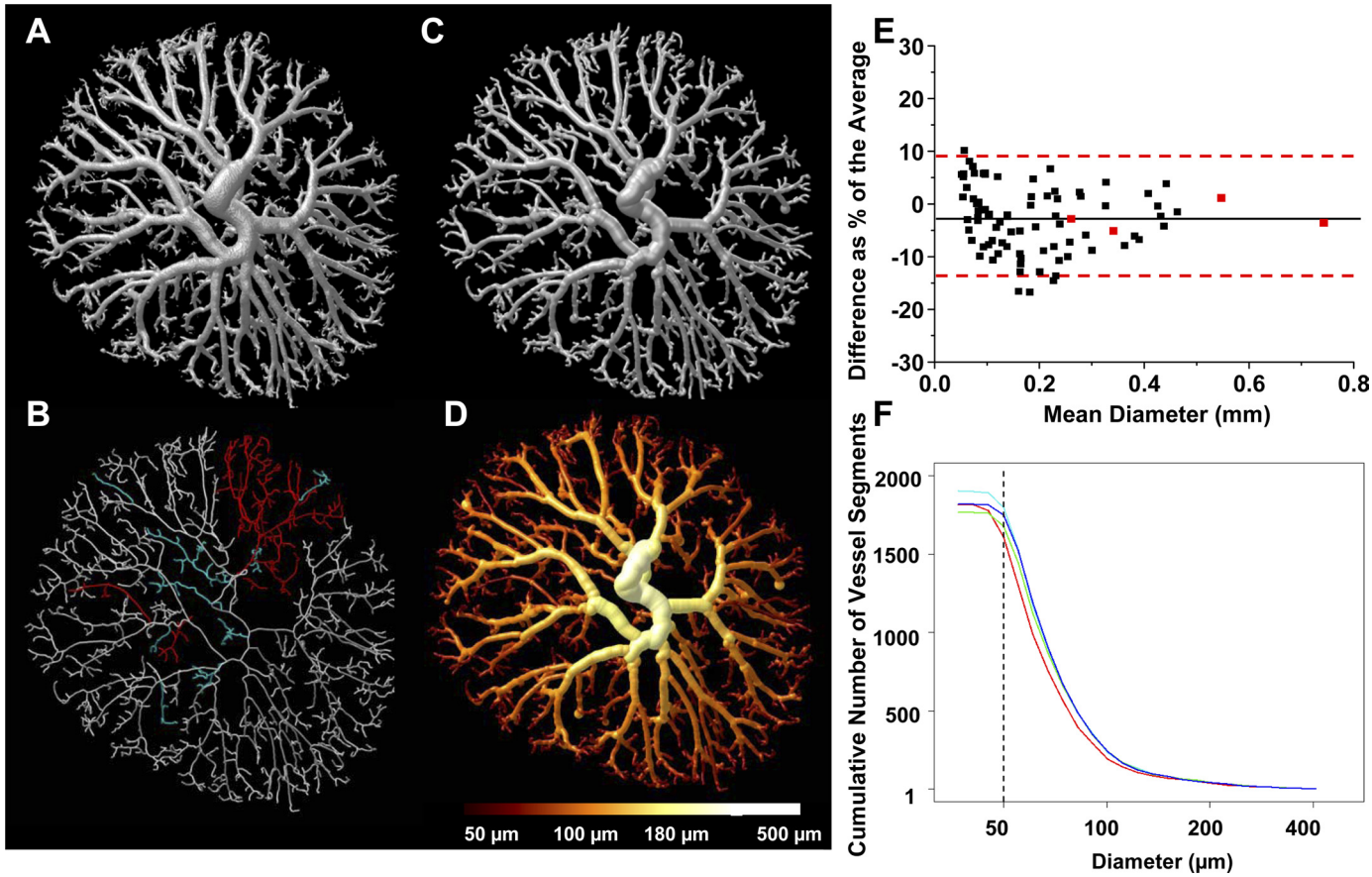

Fig. 1. Automated vascular segmentation methodology and validation. *A*: isointensity surface rendering of the fetoplacental arterial tree of a control specimen. *B*: vessel center lines generated by the vascular segmentation algorithm. The center lines shown in white were generated by the initial seed placed in the umbilical artery. Subsequent seeds were placed in vessels visible in *A* but missed by the algorithm. The second group of seeds yielded the vessels shown in red, and a final group yielded the vessels shown in cyan. *C*: a tubular model of the data is generated for which diameter, length, and connectivity of each vessel segment is known. *D*: the distribution of vessel diameters in the arterial tree. The isosurface has been color rendered to depict vessel diameters. Chorionic plate vessels (>180 μm) are displayed in yellow and white while the smaller intraplacental arteries are shown in orange and red. *E*: the difference between diameter measurements generated by the segmentation algorithm from the tubular model and those generated by manually placing digital calipers on the isointensity images was determined. The difference was expressed as a percent of the average. The percent difference was plotted vs. the mean of those two measurements to assess agreement. Measurements of placental vessels (black) and of polyethylene tubing (red) are shown. The mean bias (black line) was −2.89%, and the 95% confidence interval (red broken lines) was −15.02% to 9.24%. *F*: the cumulative number of vessel segments (*y*-axis) greater than a given diameter (*x*-axis). Curves show results for one control specimen that was scanned, segmented, and analyzed 4 times. The slopes of the curves are noticeably diminished at ~50 μm (denoted by the broken line).

difficult to detect, and therefore all subsequent analysis was performed solely on segments greater than this 50-μm-diameter threshold. The mean number of vessel segments >50 μm in the repeat scans was 1,625, with a coefficient of variation (COV) of 3%.

Hemodynamic modeling. Each tubular model was visually compared with micro-CT isosurface images to verify accurate connections. Vascular resistance was calculated based on vessel architecture through use of standard formulas for resistances in parallel and in series as described previously (59) and the viscosity of blood in small vessels based on Pries and Secomb (46). Vascular resistance measurements were found to be reproducible (range: 0.28–0.31 mmHg·s·μl^{-1}, COV = 4.2%) in the one control specimen that underwent four scan/segmentation/analysis repetitions. Datasets for which the umbilical vessel was not present due to the umbilical cord being tied off too close to the chorionic plate during the perfusion process (one control and one PAH treated) were eliminated from hemodynamic modeling analyses. The distribution of pressure and flow in the tree was calculated by assuming *1*) Poiseuille's law for flow of fluid through a pipe-like structure, *2*) equal pressure at each terminal vessel, and *3*) a diameter-dependent blood viscosity correction affecting small vessels as described in Pries and Secomb (46). Umbilical artery vessel length was set to 1 mm in each dataset to eliminate variability associated with severing this vessel. Pressure drop across the vascular bed was estimated from the calculated resistance and literature values for systolic peak blood velocity in the umbilical artery (37). For the latter, we assumed a parabolic blood velocity profile to estimate the corresponding flow rate.

Arylhydrocarbon receptor immunohistochemistry. With the use of the injection procedure described above, Microfil was perfused into either the arterial (n = 4) or venous (n = 4) fetoplacental circulation from vehicle control dams at E15.5. These placentas were then fixed in 10% buffered formalin phosphate until tissue was ready for processing, at which point placentas were embedded and sectioned using routine histological methods. Details of the antigen retrieval and staining procedures can be found in the Supplemental Methods. Tissue sections from both venous-filled (n = 4) and arterial-filled (n = 4) placentas were evaluated. Photomicrographs were taken using a Leitz DMRXE microscope, a Sony DXC-970MD camera, and Northern Eclipse software.

Statistical analysis. Paired *t*-tests were used to compare the diameter measurements generated via the segmentation algorithm with manual measurements made using digital calipers. Two-way ANOVA

was performed to evaluate effects of treatment group and litter. Although litter size did not differ by group, litter was nevertheless a strong factor in our analysis. Thus results are presented as the mean of litter averages ± SE where n is the number of litters ($n = 4$ control, $n = 5$ PAH treated). Significant P values range from 0.05 to 0.0001. All statistical tests were performed using R statistical software (www.r-project.org).

RESULTS

Control phenotype of the fetoplacental arterial tree. In control pregnancies, the fetoplacental arterial vessels branched out from a centrally located umbilical artery to form a circular tree with a span of 6.4 ± 0.08 mm and depth of 0.98 ± 0.04 mm. This structure was visualized from 3D vascular surface renderings generated from micro-CT data (Fig. 1*A*). The umbilical artery divided into vessels that branched across the surface of the chorionic plate before abruptly branching into small-diameter intraplacental arteries. Chorionic plate vessels at this branch point were typically 180 μm in diameter. This was visualized by color coding for vessel diameter (Fig. 1*D*). Arterial trees contained ~1,350 ± 114 vessel segments of which <3% were located at the chorionic surface. The branching pattern was mostly dichotomous, and the number of vessels greater than a given diameter was well described by a power law with diameter scaling coefficient of −2.89 ± 0.04. This is consistent with reports for other organs (20) and similar to the coefficient of −3 predicted by Murray's Law (20). The total length of all vessel segments was 295 ± 11 mm.

Total vascular resistance calculated based on the vascular geometry was 0.28 ± 0.01 mmHg·s·μl^{-1}. Umbilical artery diameter (d) was 0.51 ± 0.02 mm. Assuming 100 mm/s peak systolic velocity in the umbilical artery (37), a parabolic blood velocity profile (mean velocity = 1/2 peak velocity), and an average velocity (v) over the cardiac cycle corresponding to half the peak velocity, we estimated umbilical arterial blood flow to be 5.3 μl/s [i.e., $\pi(d/2)^2 \cdot v$]. Using this estimated flow, and the calculated vascular resistance for each tree, the pressure differential was calculated to be 1.49 ± 0.07 mmHg between the distal end of the umbilical artery and the smallest vessels included in the simulation (50 μm). Example images representing flow distribution for an arterial tree are shown in Fig. 5, *B* and *C*.

PAH-treated phenotype of the fetoplacental arterial tree. PAH embryos in the current study were growth restricted by 23% in weight (Table 1), whereas growth restriction was 14% in weight in a larger prior report (14). There was no significant change in litter size or placental weight in the PAH-treated group, consistent with our prior results (14).

Table 1. *Fetal and placental growth parameters*

	Controls ($n = 10$)	PAH Exposed ($n = 10$)	ANOVA (P)
Fetal wet wt, g	0.44 ± 0.06	0.34 ± 0.03	<0.0001
Placental wt, g	0.15 ± 0.01	0.15 ± 0.01	NS
Litter size	8.8 ± 0.5	7.0 ± 0.8	NS
Vascular span, mm	6.38 ± 0.08	6.38 ± 0.11	NS
Vascular depth, mm	0.98 ± 0.04	1.03 ± 0.02	NS
Diameter scaling coefficient	−2.89 ± 0.04	−2.90 ± 0.06	NS

Values are shown as means ± SE; n, no. of specimens. PAH, polycyclic aromatic hydrocarbon; NS, not significant.

The effects of PAHs on fetal growth are mediated by arylhydrocarbon receptor (AhR) (14). We therefore mapped the expression of this protein in the placental vasculature using immunohistochemistry. AhR has previously been shown to be variably expressed specifically by endothelial cells in the mouse placenta (14, 23). AhR immunostaining was strong in the endothelium of capillaries and arterioles, moderate in the endothelium of small arteries (Fig. 2*A*), and weak in the endothelium of the largest arteries of the chorionic plate (data not shown). Little or no immunoreactivity for AhR was observed in the endothelium of veins (Fig. 2*B*). The absence of AhR in venous endothelium may explain why PAHs had no effect on the fetoplacental venous vasculature in prior work (14). Higher AhR expression by capillaries and arterioles may explain why they are more strikingly affected by PAH exposure (Ref. 14 and described below).

Large vessels of fetoplacental trees in the PAH-exposed group sometimes exhibited marked curvature when 3D vascular surface renderings were visually assessed (e.g., Fig. 3, *B* and *C*), a feature that was not observed in the control group. To quantify vessel curvature, we determined the ratio of vascular path length to the Euclidian (i.e., beeline) distance from the umbilical artery to each terminal vessel (Fig. 3*C*). There was an observable shift toward larger tortuousity ratios in the PAH-exposed group (Fig. 3*D*). The median ratio was significantly elevated in the PAH-exposed group (1.80 ± 0.04) compared with controls (1.64 ± 0.03, $P = 0.001$), suggesting that PAH exposure increased tortuousity of fetoplacental arteries and arterioles.

Branching pattern was evaluated using the diameter scaling coefficient (i.e., the relationship between parent and daughter vessel diameters) and by the segment length-to-diameter ratio. There was no change in the diameter scaling coefficient (Table 1), suggesting that the dichotomous branching pattern was similar between groups. The segment length-to-diameter ratio was also unchanged between the groups (Table 1). However, the number of arterial vessel segments was significantly reduced in the PAH-exposed group (1,113 ± 142) compared with controls (1,342 ± 114, $P < 0.01$). Distributions of the cumulative number of vessel segments greater than a certain diameter demonstrate a separation between the control and PAH-exposed groups, with the PAH-exposed curve rising less steeply toward the small-diameter range (Fig. 4*A*), indicating reductions in the number of small-diameter vessels in the tree. Interestingly, these curves begin to separate at ~180 μm in diameter, which we found to be the diameter boundary between intraplacental and chorionic plate vessels in both the control and PAH-exposed specimens. The number of intraplacental arteries (i.e., vessels ≤180 μm in diameter) was reduced by 17% in the PAH-exposed group ($P < 0.01$). This was due primarily to a 27% reduction in the number of vessel segments 50–100 μm in diameter ($P < 0.01$, Fig. 4*B*). The number of larger-diameter intraplacental vessels (100–180 μm) and chorionic plate vessels was not significantly different between the two groups. The number of terminal vessels in the tree was reduced by 13% ($P < 0.05$, Fig. 4*C*). Despite these alterations in vascularity, the depth and the span of the arterial trees were unchanged in PAH-treated mice (Table 1). This implies that the PAH-treated vascular tree has a similar branching pattern within a similarly sized labyrinthine volume but is more sparsely branched.

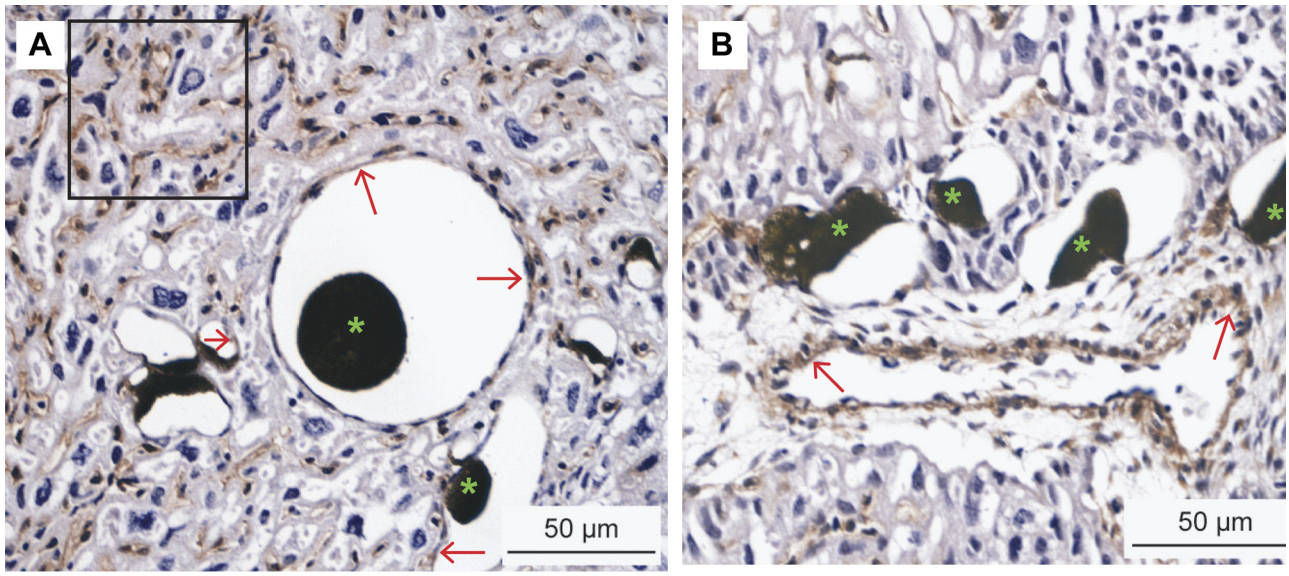

Fig. 2. Arylhydrocarbon receptor (AhR) Immunostaining. Histological sections of the placental labyrinth region of control placentas at *embryonic day* (E) *15.5*. Either the arterial (*A*) or venous (*B*) vessels were infused with Microfil (stained dark brown, examples marked with green asterisk) to mark vessel type in histological sections. Microfil does not fill the vessel lumens because of its shrinkage during histological processing. *A*: in this arterial-perfused specimen, red arrows point to brown staining for AhR in the arterial endothelium. AhR staining is also abundant in the capillaries (e.g., highlighted by black box). *B*: there was little or no staining in the endothelium of venous vessels as shown in this venous-filled specimen. In contrast, an adjacent artery has strong endothelial staining around the entire vessel (red arrows).

A sparser vascular tree in placentas from PAH-treated mothers was anticipated to result in significantly elevated vascular resistance. Indeed, calculated vascular resistance was increased by 30% compared with controls ($P = 0.015$, Fig. 5*A*). Based on the assumption that the pressure differential across the tree was the same in control and PAH groups, mean umbilical blood flow was calculated to be 4.4 ± 0.6 μl/s in the PAH-exposed group. This was significantly lower than our estimated blood flow of 5.3 μl/s in controls ($P = 0.01$).

DISCUSSION

The current study used automated vascular segmentation and computational flow calculations to quantitatively evaluate vascular morphology and hemodynamics in the fetoplacental arterial tree of the mouse. Our prior work on the PAH mouse model indicated that prepregnancy PAH exposure appeared to increase arterial tortuosity based on visual assessment of images and significantly decreased surface area and volume of the fetoplacental tree (14). Here we used automated vascular segmentation to quantify tortuosity and demonstrate the statistical significance of this change, and to determine the topological changes in the tree that caused the reduction in area and volume. We report the novel findings that the reduction in the area and volume of the tree was primarily caused by a 27% reduction in the number of arteriole-sized vessels (50–100 μm) and that larger vessels were relatively spared. Also novel were the observations that changes in vascularity were not caused by changes in the overall size of the tree (i.e., its depth or span), or marked changes in the branching pattern itself (i.e., no change in the scaling coefficient or length-to-diameter ratio). Our quantification of the topology of the tree was used to estimate the impact of these changes on vascular resistance and flow. Changes in vascular geometry were predicted to lead to a 30% increase in fetoplacental arterial vascular resistance. Thus we show novel statistically and physiologically significant differences between arterial fetoplacental vascular trees in control vs. PAH-exposed pregnancies.

Automation in the current study meant that larger numbers of specimens could be analyzed, permitting intra- and intergroup statistical comparisons. This contrasts with most previous vascular segmentation studies that report data for small sample numbers (e.g., $n = 1$–3), where intergroup statistical comparisons were not performed (26, 40, 41). Our automated results show that vascular segmentation was highly reproducible (within 3%). The average percent difference between manual and segmentation-generated vessel diameters was <3%, and >97% of the tree's originally imaged volume was present in the segmented, reconstructed vascular trees. The novel physiological results we present demonstrate the ability of vascular segmentation to pinpoint specific vascular insults in the fetoplacental circulation, enhance our understanding of fetoplacental vascular structure, and reveal the effects of PAH exposure on this developing vascular tree.

Characterization of the fetoplacental vascular tree in normal pregnancy. During normal development, the fetoplacental vasculature undergoes extensive morphogenesis, angiogenesis, and vascular remodeling as it grows and branches into a low-resistance vascular tree. This tree must have adequate surface area for nutrient exchange with the maternal blood that circulates through adjacent maternal blood spaces of the labyrinth. By E15.5, there is an elaborate vascular tree structure in place consisting on average of 1,350 vessel segments >50 μm in diameter. These segments total 0.295 meters of vasculature, yet feed more than 24 meters of capillaries in the labyrinth at this stage of development (10). Murine fetoplacental capillaries have been quantitatively evaluated from histological sections

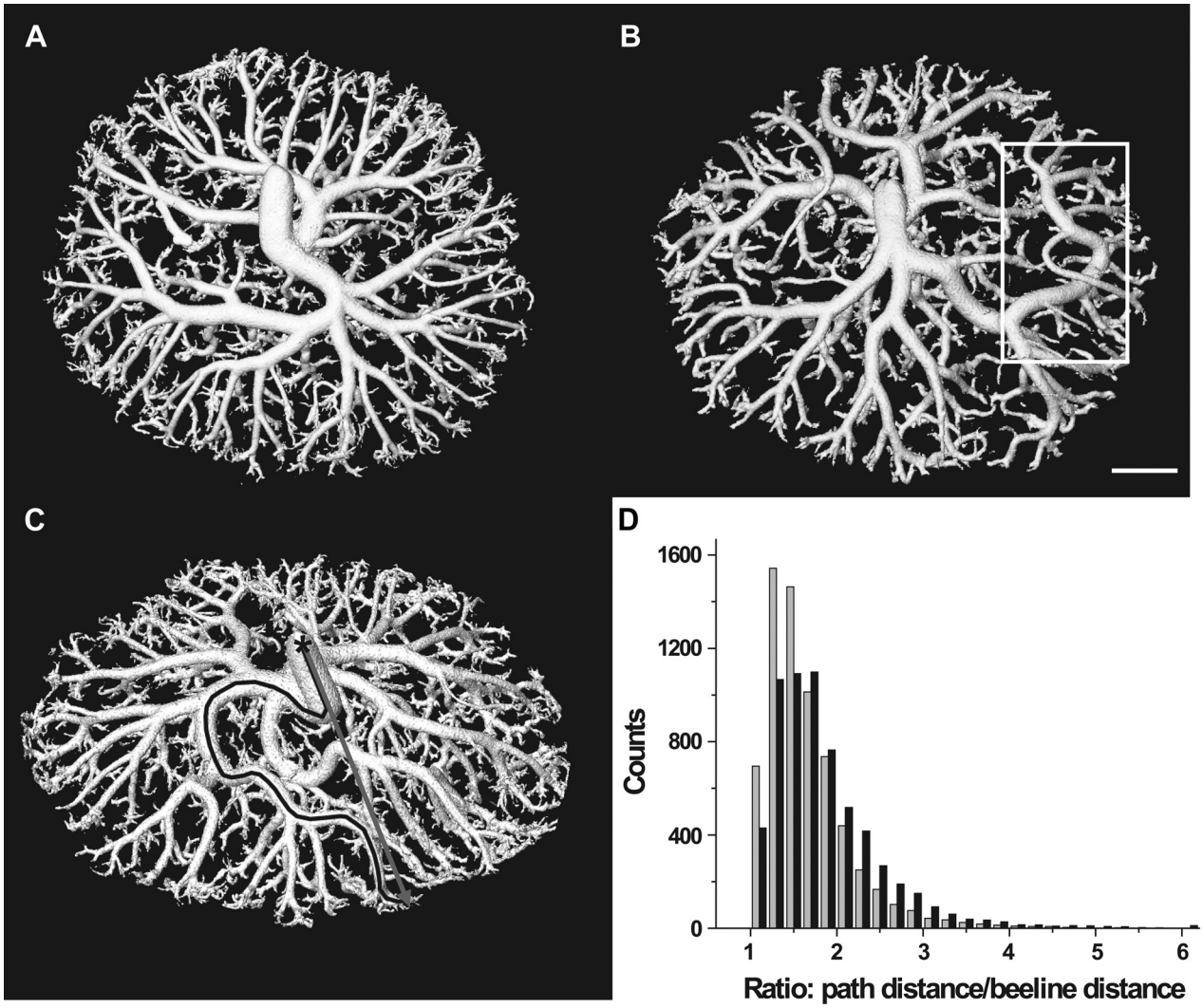

Fig. 3. Vascular tortuousity. Example isosurface renderings are shown for control (*A*) and polycyclic aromatic hydrocarbon (PAH)-exposed (*B* and *C*) specimens. *B*: pronounced vessel curvature was observed in some PAH-exposed specimens (e.g., in white box). *C*: vessel tortuousity was quantified as the ratio of the vascular path length (black line) to the beeline distance (gray arrow) from the umbilical artery (asterisk) to each terminal vessel. *D*: a histogram of the vessel tortuousity ratio for all vessels in all specimens demonstrates a skewed histogram toward larger tortuousity ratios in the PAH-exposed group (black bars) compared with controls (gray bars). Two-way ANOVA was performed to evaluate effects of treatment group and litter on the median tortuousity ratio. All three images have a scale indicated by the scale bar in *B* (1 mm).

using stereology (10), but there are no prior reports quantifying vessels in our reported diameter range.

Hemodynamics plays an important role in controlling the growth of vascular networks, laying down a branching structure that ultimately determines resistance to flow. Vascular resistance is determined by the size of individual vessels and their organization within a vascular network, and by blood viscosity and vascular tone. Blood flow in the fetoplacental vasculature was modeled as laminar since the low flow velocities (37) and small diameters of the vessels result in a low Reynolds number [Re $<$500 (45)] that is well below the threshold for turbulent flow [Re $>$2,000 (39)]. Hematocrit levels are unaltered after low-dose PAH exposure (6); thus, viscosity was modeled similarly in both control and PAH mice using a correction factor for adult blood viscosity changes in small vessels (46). Viscosity of fetal blood may be higher given that fetal red blood cells at this gestational time point are much larger than adult cells (22). Resting tone is low in the fetoplacental tree (42). Our previous work comparing umbilical artery diameters from ex vivo micro-CT with in vivo ultrasound observed no difference (47), suggesting that fetoplacental vessels are maximally dilated in vivo and that vascular tone is unaltered by our ex vivo perfusions.

The total resistance across the fetoplacental arterial vasculature averaged 0.28 mmHg·s·μl^{-1}. It is important to note that umbilical artery pressure and blood velocity were not measured in our study and that calculations of resistance are estimates only. Estimation of fetoplacental arterial vascular resistance in the mouse is novel, and, as such, there are no literature values with which to assess its accuracy. However, we can evaluate our previously reported measurement of adult lung arterial vascular resistance [r = 0.029 mmHg·s·μl^{-1} (59)], obtained using the same methodology reported herein, with accepted literature values of pulmonary artery pressure (ΔP = 16.4 mmHg) (54) and cardiac ouput (q = 277 μl/s) (19) to demonstrate that our measurements of pulmonary resistance (r =

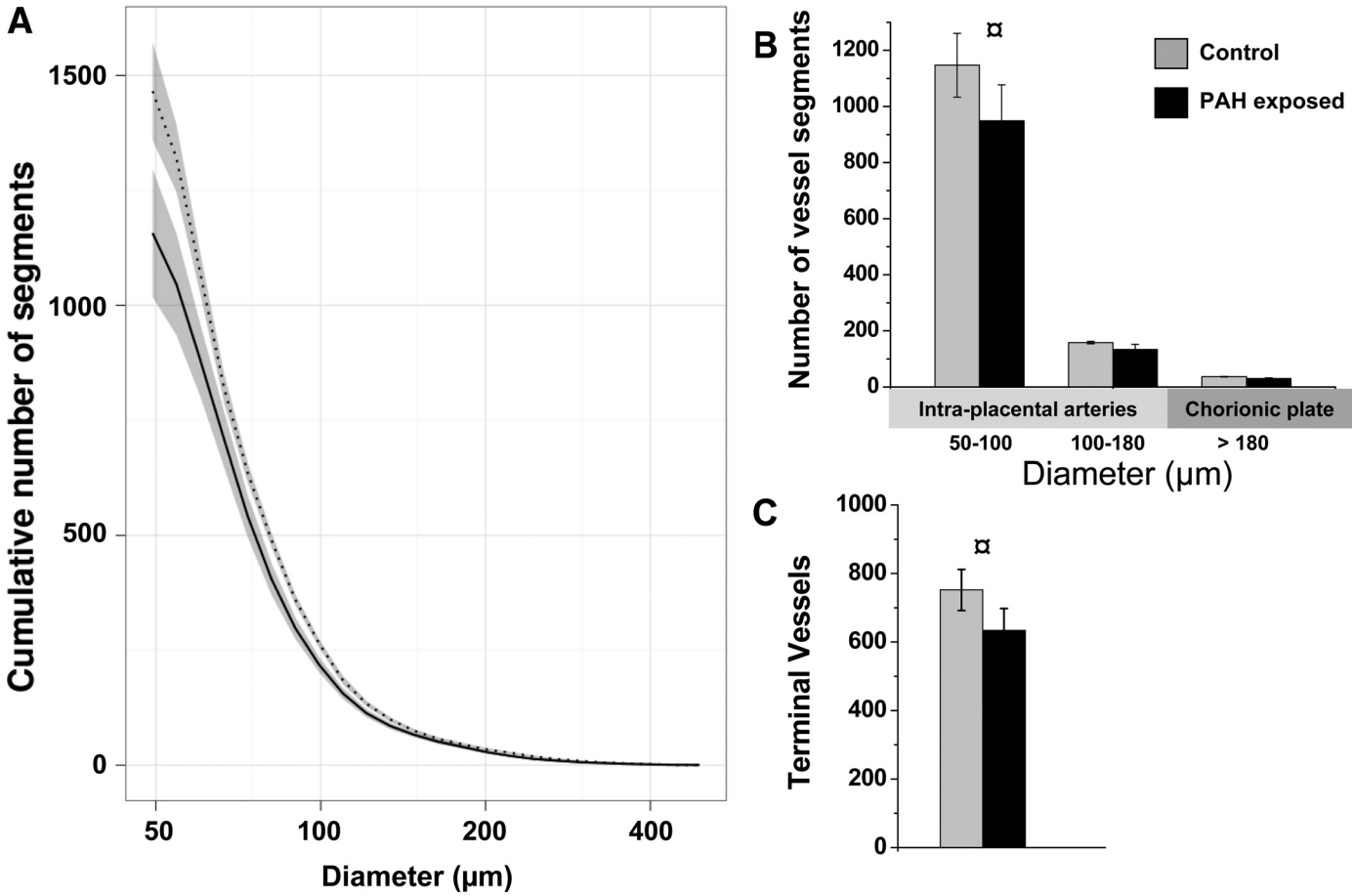

Fig. 4. Number of vessel segments. *A*: cumulative distributions of vessel diameters for the PAH-exposed group mean (solid line, shading shows ± SE) compared with controls (hatched line). The SE band is noticeably larger for the PAH-exposed curve because of the larger variation within that group. *B*: the number of vessel segments within 3 diameter ranges (50–100, 100–180, and >80 μm). *C*: the number of terminal vessels are shown for PAH-exposed (black bars, $n = 10$) and control (gray bars, $n = 10$) specimens. Data are shown as means ± SE. ¤Significant difference ($P < 0.05$) between groups.

Δp/q) are within a factor of two of the accepted value (0.059 mmHg·s·μl^{-1}). Our estimated fetoplacental arterial resistance is 10 times higher than that of the lung. This is not unexpected at the stage of gestation examined. The lung is an extremely low-resistance, fully developed adult vascular bed containing >3,000 arterial vessel segments (59). Comparatively, the E15.5 fetoplacental arterial vasculature has almost three times fewer vessel segments and was not fully mature. We speculate that the more mature fetoplacental vasculature in later gestation would have significantly lower arterial vascular resistance than reported here because of its more elaborate branching (47).

By combining our resistance calculations with murine umbilical blood velocity values obtained from the literature (27, 37), we calculated that the average pressure differential from the umbilical artery to the smallest vessels used in our simulations (50 μm) was 1.49 mmHg. Cardiac intraventricular peak systolic pressure in mouse embryos at E14.5 is 11 mmHg (18). We would expect the pressure differential across the fetoplacental arterial tree to represent a small portion of this total gradient due to pressure differentials across the upstream aorta, iliac artery and umbilical artery, and downstream arterioles (i.e., <50 μm), capillaries, and the venous circulation. At a similar stage in the rat, umbilical artery pressure is 3.6 mmHg (38), suggesting that <40% of the pressure differential across the circulation is lost downstream of the umbilical artery. Thus our results suggesting ~15% of this total pressure differential occurs across the fetoplacental arterial tree would appear reasonable. We are aware of no other data with which to compare our results.

PAH-exposed phenotype. Prepregnancy PAH exposure in our mouse model caused a 17% reduction in the total number of intraplacental fetal arteries (<180 μm) primarily because of a reduction in the number of small-diameter (50–100 μm) intraplacental arterial vessels. This decrease presumably accounts for the 20% decrease in arterial vascular volume we previously reported in this model (14). The effects of smoking on vessels in this diameter range (>50 μm) have not previously been evaluated. However, our results in arterioles are consistent with prior studies on the effects of smoking on capillaries. After exposure to cigarette smoke, the capillaries of the human placenta, chick chorioallantoic membranes, and mouse hindlimb each exhibited reduced vascular branching or volume (25, 31, 32). In contrast, our prepregnancy PAH exposure model resulted in an apparent increase in capillaries (14), as does prepregnancy exposure of mice to environmental pollutants (55). This could suggest compensatory growth of capillaries occurs in the placentas of mice but not humans. In mice, the number of chorionic plate vessels (>180 μm) was

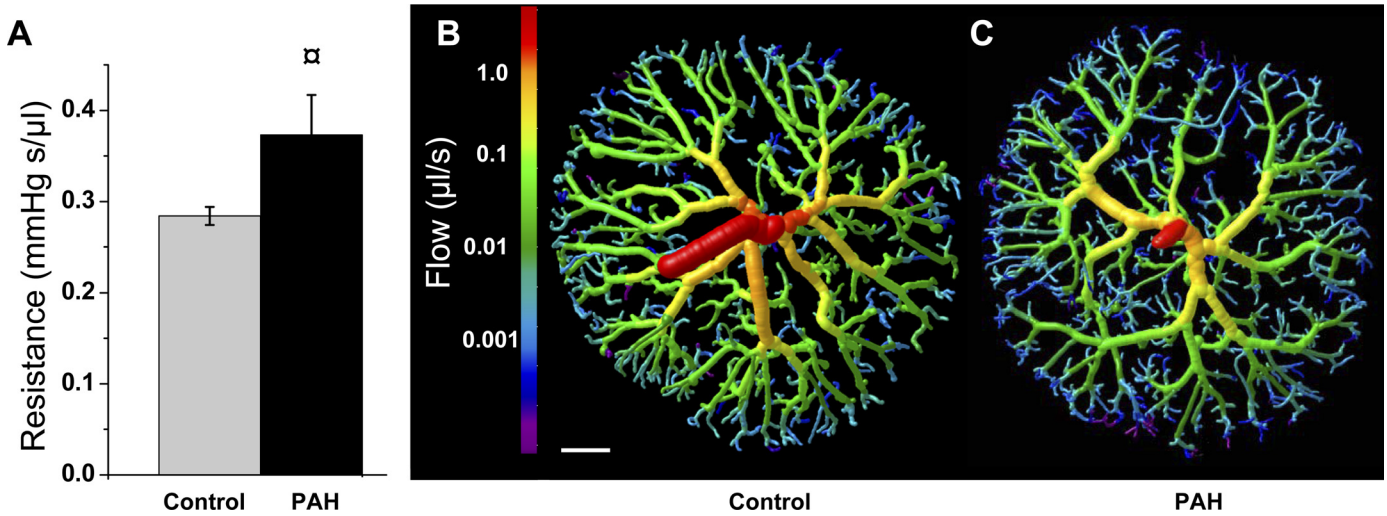

Fig. 5. Vascular hemodynamics. *A*: total vascular resistance of the fetoplacental arterial tree of PAH-exposed (black bars, $n = 9$) and control (gray bars, $n = 9$) placentas. Data are shown as means ± SE. Two-way ANOVA was performed to evaluate effects of treatment group and litter on total vascular resistance. *P* value shown represents a significant effect of treatment. ¤$P = 0.015$. Vascular resistance at each site in the tree was determined by vessel diameter and connectivity. A constant pressure gradient across all arterial trees was used to calculate blood flow from vascular resistance. *B* and *C*: isosurfaces were color rendered to illustrate blood flow magnitude (shown on logarithmic scale) in example control (*B*) and PAH-exposed (*C*) placentas. The trees of PAH-exposed placentas had lower flows throughout. This was most noticeable at the terminal vessels, which display more blue coloring compared with controls. Scale bar = 1 mm.

unchanged in PAH-exposed placentas. Chorionic plate branching morphogenesis may be less affected due to lower expression of AhR, which mediates the effects of PAHs on fetal growth (14), and/or these larger vessels may be under tighter genetic control and therefore less susceptible to environmental effects, including PAH exposure.

Our findings of reduced vascular branching are especially interesting given that vascular span and depth were unchanged in PAH-exposed placentas, suggesting that the tree is not smaller in overall size, rather that it is sparse. A constant placental size is supported by unaltered placental weight measurements in the PAH-treated group. Numerous human studies of maternal smoking also found that placental weight is unaltered (3, 25).

Prepregnancy PAH exposure in our mouse model led to increased tortuousity in the larger arteries of the fetoplacental tree. We previously noted increased tortuousity in the PAH-exposed capillary bed when imaged using vascular corrosion casts (14). Increased capillary tortuousity in the microcirculations of human smokers (50) and chick membranes exposed to cigarette smoke (31) support these results. The mechanisms causing increased vessel tortuousity are unknown. In the rapidly developing tumor vasculature, coiling is often attributed to rapid vessel growth due to hypoxia, an imbalance of angiogenic factors, and/or altered response to growth promotion signals (57). Changes may also be due in part to effects of PAHs on the extracellular matrix (ECM). The ECM plays an important role in regulating angiogenesis and vascular modeling. Decreased collagen distribution in placentas from PAH-exposed mothers (14) is consistent with studies reporting reduced collagen secretion from smooth muscle cells cultured in the presence of these chemicals (53). Because collagen is thought to provide a substrate for endothelial cell migration, such dysregulation of ECM proteins may lead to poorly formed vasculature. Altered ECM has been linked to erratic vasculature in tumors (4) and in chick chorionic membranes exposed to cigarette smoke (31). Thus, reduced collagen deposition may have led to an ineffective substrate for laying down a branching structure, leading to tortuous vessels and potentially also to reduced vessel numbers.

Computational flow calculations predict that the observed differences in the fetoplacental vascular tree would significantly increase vascular resistance. Based on vascular geometry, we found total resistance to blood flow in our growth-restricted mouse model to be elevated by ~30%. Assuming umbilical artery pressure is unchanged by PAH exposure, this resistance increase would correspond to a 19% decrease in umbilical blood flow. This decrease is very similar to our observed decrease in PAH-exposed fetal weight (23%). However, it should be noted that umbilical artery pressure was not directly measured in this study; thus, our estimation of PAH-exposed blood flow may be inaccurate. Additionally, there may be other contributing factors to fetal weight restriction. Reductions in umbilical blood flow reduce fetal oxygen consumption and therefore can lead to growth restriction (2); however, uteroplacental vascular deficits, reduced nutrient transport, increased interhemal membrane thickness, and decreased diffusion capacity can each restrict fetal growth (52). In addition, PAHs may act directly on the embryo to negatively affect its growth. Certainly PAHs are able to cross the perfused human placenta in vitro (30), and high doses given to pregnant rats cause fetal vascular hemorrhage (49). These results suggest that PAH exposure can have direct fetal effects. Thus the direct effects of PAHs on the fetus, uteroplacental vasculature, and placental function warrant further study.

Segment numbers, degree of tortuousity, and vascular resistance were all significantly affected by litter. This was not due to any differences in litter size. Rather this suggests that mothers reacted differently to the PAH treatment regime. In humans, the effects of smoking are also highly variable. Maternal smoking does not lead to fetal growth restriction in all pregnancies, nor is the reduced capillary phenotype present in

all cases (e.g., see Ref. 44). There is evidence that the effect of smoking on fetal birth weight in humans can be modified by maternal genotype, including that of CYP1A1 (56), which is an AhR-regulated protein involved in the conversion of toxic PAHs to less harmful substances. We have also observed disparities in the degree of growth restriction between two mouse strains, C57Bl6 and CD1, given the identical PAH treatment regimen (13, 14). These differences may be due to AhR, which is highly polymorphic among mouse strains (28) and mediates the effects of PAH on fetal growth (14). The current study used an inbred strain to control for genetic variability. However, there may be epigenetic differences between animals due to different environmental influences. Some variability also could be attributed to contamination of the fur during injection that would tend to increase the dose received by high-grooming mice. The severity of the small vessel count was not correlated with the number of days between injection and conception (data not shown), so this factor did not appear to explain interlitter variability.

In conclusion, automated vascular segmentation of micro-CT datasets and computational flow calculations were used to generate quantitative parameters describing the murine arterial fetoplacental vascular tree, including vascular tortuosity, branching pattern, and distribution of vessel diameters. From these data, we estimated effects on resistance and blood flow. Results show that prepregnancy PAH exposure led to a significant reduction in the number of small-diameter intraplacental vessels, but not in the number of larger-diameter chorionic plate vessels, demonstrating the ability of vascular segmentation to elucidate specific vascular insults in the fetoplacental arterial tree. PAH-exposed trees also exhibited an increase in vascular tortuosity. Results predict that such changes in vascular geometry would lead to a 30% increase in arterial vascular resistance and hence are physiologically significant. The wide applicability of our approach suggests that it will serve as a key analysis tool in the study of various vascular beds in genetically altered mice, other animal models, and in humans.

GRANTS

This work was funded by Heart and Stroke Foundation of Ontario Grants NA5804 and T6297 and Canadian Institute of Health Research Grant MOP86734. M. Y. Rennie was funded by an Ontario Graduate Scholarship. S. L. Adamson gratefully acknowledges support as the Anne and Max Tanenbaum Chair in Molecular Medicine at Mount Sinai Hospital.

DISCLOSURES

No conflicts of interest are declared by the authors.

REFERENCES

1. **Albuquerque CA, Smith KR, Johnson C, Chao R, Harding R.** Influence of maternal tobacco smoking during pregnancy on uterine, umbilical and fetal cerebral artery blood flows. *Early Hum Dev* 80: 31–42, 2004.
2. **Anderson DF, Parks CM, Faber JJ.** Fetal O2 consumption in sheep during controlled long-term reductions in umbilical blood flow. *Am J Physiol Heart Circ Physiol* 250: H1037–H1042, 1986.
3. **Benirschke K, Kaufmann P, Baergen RN.** *Pathology of the Human Placenta*. New York, NY: Springer, 2006.
4. **Bergers G, Brekken R, McMahon G, Vu TH, Itoh T, Tamaki K, Tanzawa K, Thorpe P, Itohara S, Werb Z, Hanahan D.** Matrix metalloproteinase-9 triggers the angiogenic switch during carcinogenesis. *Nat Cell Biol* 2: 737–744, 2000.
5. **Bernstein IM, Plociennik K, Stahle S, Badger GJ, Secker-Walker R.** Impact of maternal cigarette smoking on fetal growth and body composition. *Am J Obstet Gynecol* 183: 883–886, 2000.
6. **Booker CD, White KL Jr.** Benzo(a)pyrene-induced anemia and splenomegaly in NZB/WF1 mice. *Food Chem Toxicol* 43: 1423–1431, 2005.
7. **Bridgewater D, Rosenblum ND.** Stimulatory and inhibitory signaling molecules that regulate renal branching morphogenesis. *Pediatr Nephrol* 24: 1611–1619, 2009.
8. **Burton GJ, Palmer ME, Dalton KJ.** Morphometric differences between the placental vasculature of non-smokers, smokers and ex-smokers. *Br J Obstet Gynaecol* 96: 907–915, 1989.
9. **Cnattingius S.** The epidemiology of smoking during pregnancy: smoking prevalence, maternal characteristics, and pregnancy outcomes. *Nicotine Tob Res* 6, *Suppl* 2: S125–S140, 2004.
10. **Coan PM, Ferguson-Smith AC, Burton GJ.** Developmental dynamics of the definitive mouse placenta assessed by stereology. *Biol Reprod* 70: 1806–1813, 2004.
11. **Colman GJ, Joyce T.** Trends in smoking before, during, and after pregnancy in ten states. *Am J Prev Med* 24: 29–35, 2003.
12. **Coultas L, Chawengsaksophak K, Rossant J.** Endothelial cells and VEGF in vascular development. *Nature* 438: 937–945, 2005.
13. **Detmar J, Rabaglino T, Taniuchi Y, Oh J, Acton BM, Benito A, Nunez G, Jurisicova A.** Embryonic loss due to exposure to polycyclic aromatic hydrocarbons is mediated by Bax. *Apoptosis* 11: 1413–1425, 2006.
14. **Detmar J, Rennie MY, Whiteley KJ, Qu D, Taniuchi Y, Shang X, Casper RF, Adamson SL, Sled JG, Jurisicova A.** Fetal growth restriction triggered by polycyclic aromatic hydrocarbons is associated with altered placental vasculature and AhR-dependent changes in cell death. *Am J Physiol Endocrinol Metab* 295: E519–E530, 2008.
15. **Fridman Y, Pizer SM, Aylward S, Bullitt E.** Extracting branching tubular object geometry via cores. *Med Image Anal* 8: 169–176, 2004.
16. **Gladen BC, Zadorozhnaja TD, Chislovska N, Hryhorczuk DO, Kennicutt MC, Little RE.** Polycyclic aromatic hydrocarbons in placenta. *Hum Exp Toxicol* 19: 597–603, 2000.
17. **Hoffmann D, Hoffmann I.** The changing cigarette, 1950–1995. *J Toxicol Environ Health* 50: 307–364, 1997.
18. **Ishiwata T, Nakazawa M, Pu WT, Tevosian SG, Izumo S.** Developmental changes in ventricular diastolic function correlate with changes in ventricular myoarchitecture in normal mouse embryos. *Circ Res* 93: 857–865, 2003.
19. **Janssen B, Debets J, Leenders P, Smits J.** Chronic measurement of cardiac output in conscious mice. *Am J Physiol Regul Integr Comp Physiol* 282: R928–R935, 2002.
20. **Kassab GS.** Scaling laws of vascular trees: of form and function. *Am J Physiol Heart Circ Physiol* 290: H894–H903, 2006.
21. **Kimya Y, Cengiz C, Ozan H, Kolsal N.** Acute Effects of Maternal Smoking on the Uterine and Umbilical Artery Blood Velocity Waveforms. *J Matern Fetal Investig* 8: 79–81, 1998.
22. **Kingsley PD, Malik J, Fantauzzo KA, Palis J.** Yolk sac-derived primitive erythroblasts enucleate during mammalian embryogenesis. *Blood* 104: 19–25, 2004.
23. **Kitajima M, Khan KN, Fujishita A, Masuzaki H, Koji T, Ishimaru T.** Expression of the arylhydrocarbon receptor in the peri-implantation period of the mouse uterus and the impact of dioxin on mouse implantation. *Arch Histol Cytol* 67: 465–474, 2004.
24. **Kulandavelu S, Qu D, Sunn N, Mu J, Rennie MY, Whiteley KJ, Walls JR, Bock NA, Sun JC, Covelli A, Sled JG, Adamson SL.** Embryonic and neonatal phenotyping of genetically engineered mice. *ILAR J* 47: 103–117, 2006.
25. **Larsen LG, Clausen HV, Jonsson L.** Stereologic examination of placentas from mothers who smoke during pregnancy. *Am J Obstet Gynecol* 186: 531–537, 2002.
26. **Lee J, Beighley P, Ritman E, Smith N.** Automatic segmentation of 3D micro-CT coronary vascular images. *Med Image Anal* 11: 630–647, 2007.
27. **MacLennan MJ, Keller BB.** Umbilical arterial blood flow in the mouse embryo during development and following acutely increased heart rate. *Ultrasound Med Biol* 25: 361–370, 1999.
28. **Maier A, Micka J, Miller K, Denko T, Chang CY, Nebert DW, Alvaro P.** Aromatic hydrocarbon receptor polymorphism: development of new methods to correlate genotype with phenotype. *Environ Health Perspect* 106: 421–426, 1998.
29. **Mathews TJ.** Smoking during pregnancy in the 1990s. *Natl Vital Stat Rep* 49: 1–14, 2001.
30. **Mathiesen L, Rytting E, Mose T, Knudsen LE.** Transport of benzoαpyrene in the dually perfused human placenta perfusion model: effect of albumin in the perfusion medium. *Basic Clin Pharmacol Toxicol* 105: 181–187, 2009.

31. **Melkonian G, Le C, Zheng W, Talbot P, Martins-Green M.** Normal patterns of angiogenesis and extracellular matrix deposition in chick chorioallantoic membranes are disrupted by mainstream and sidestream cigarette smoke. *Toxicol Appl Pharmacol* 163: 26–37, 2000.
32. **Michaud SE, Menard C, Guy LG, Gennaro G, Rivard A.** Inhibition of hypoxia-induced angiogenesis by cigarette smoke exposure: impairment of the HIF-1alpha/VEGF pathway. *FASEB J* 17: 1150–1152, 2003.
33. **Modica R, Fiume M, Guaitani A, Bartosek I.** Comparative kinetics of benz(a)anthracene, chrysene and triphenylene in rats after oral administration. I. Study with single compounds. *Toxicol Lett* 18: 103–109, 1983.
34. **Mooney LA, Santella RM, Covey L, Jeffrey AM, Bigbee W, Randall MC, Cooper TB, Ottman R, Tsai WY, Wazneh L.** Decline of DNA damage and other biomarkers in peripheral blood following smoking cessation. *Cancer Epidemiol Biomarkers Prev* 4: 627–634, 1995.
35. **Morrisey EE, Hogan BL.** Preparing for the first breath: genetic and cellular mechanisms in lung development. *Dev Cell* 18: 8–23, 2010.
36. **Morrow RJ, Ritchie JW, Bull SB.** Maternal cigarette smoking: the effects on umbilical and uterine blood flow velocity. *Am J Obstet Gynecol* 159: 1069–1071, 1988.
37. **Mu J, Adamson SL.** Developmental changes in hemodynamics of the uterine artery, the utero- and umbilico-placental, and vitelline circulations in the mouse throughout gestation. *Am J Physiol Heart Circ Physiol* 291: H1421–H1428, 2006.
38. **Nakazawa M, Miyagawa S, Ohno T, Miura S, Takao A.** Developmental hemodynamic changes in rat embryos at 11 to 15 days of gestation: normal data of blood pressure and the effect of caffeine compared to data from chick embryo. *Pediatr Res* 23: 200–205, 1988.
39. **Nichols WW.** *McDonald's Blood Flow in Arteries: Theoretical, Experimental and Clinical Principles*. Oxford, UK: Oxford Univ Press, 2006.
40. **Nordsletten DA, Blackett S, Bentley MD, Ritman EL, Smith NP.** Structural morphology of renal vasculature. *Am J Physiol Heart Circ Physiol* 291: H296–H309, 2006.
41. **Op Den BJ, Bajzer Z, Ritman EL.** Branching morphology of the rat hepatic portal vein tree: a micro-CT study. *Ann Biomed Eng* 34: 1420–1428, 2006.
42. **Paulick RP, Meyers RL, Rudolph AM.** Vascular responses of umbilical-placental circulation to vasodilators in fetal lambs. *Am J Physiol Heart Circ Physiol* 261: H9–H14, 1991.
43. **Perera FP, Jedrychowski W, Rauh V, Whyatt RM.** Molecular epidemiologic research on the effects of environmental pollutants on the fetus. *Environ Health Perspect* 107, *Suppl* 3: 451–460, 1999.
44. **Pfarrer C, Macara L, Leiser R, Kingdom J.** Adaptive angiogenesis in placentas of heavy smokers (Abstract). *Lancet* 354: 303, 1999.
45. **Phoon CK, Aristizabal O, Turnbull DH.** Spatial velocity profile in mouse embryonic aorta and Doppler-derived volumetric flow: a preliminary model. *Am J Physiol Heart Circ Physiol* 283: H908–H916, 2002.
46. **Pries AR, Secomb TW.** Rheology of the microcirculation. *Clin Hemorheol Microcirc* 29: 143–148, 2003.
47. **Rennie MY, Whiteley KJ, Kulandavelu S, Adamson SL, Sled JG.** 3D visualisation and quantification by microcomputed tomography of late gestational changes in the arterial and venous feto-placental vasculature of the mouse. *Placenta* 28: 833–840, 2007.
48. **Salafia C, Shiverick K.** Cigarette smoking and pregnancy II: vascular effects. *Placenta* 20: 273–279, 1999.
49. **Sanyal MK, Li YL.** Deleterious effects of polynuclear aromatic hydrocarbon on blood vascular system of the rat fetus. *Birth Defects Res B Dev Reprod Toxicol* 80: 367–373, 2007.
50. **Scardina GA.** The effect of cigar smoking on the lingual microcirculation. *Odontology* 93: 41–45, 2005.
51. **Schneider S, Huy C, Schutz J, Diehl K.** Smoking cessation during pregnancy: a systematic literature review. *Drug Alcohol Rev* 29: 81–90, 2010.
52. **Sibley CP, Turner MA, Cetin I, Ayuk P, Boyd CA, D'Souza SW, Glazier JD, Greenwood SL, Jansson T, Powell T.** Placental phenotypes of intrauterine growth. *Pediatr Res* 58: 827–832, 2005.
53. **Stavenow L, Pessah-Rasmussen H.** Effects of polycyclic aromatic hydrocarbons on proliferation, collagen secretion and viability of arterial smooth muscle cells in culture. *Artery* 15: 94–108, 1988.
54. **Steudel W, Ichinose F, Huang PL, Hurford WE, Jones RC, Bevan JA, Fishman MC, Zapol WM.** Pulmonary vasoconstriction and hypertension in mice with targeted disruption of the endothelial nitric oxide synthase (NOS 3) gene. *Circ Res* 81: 34–41, 1997.
55. **Veras MM, Damaceno-Rodrigues NR, Caldini EG, Maciel Ribeiro AA, Mayhew TM, Saldiva PH, Dolhnikoff M.** Particulate urban air pollution affects the functional morphology of mouse placenta. *Biol Reprod* 79: 578–584, 2008.
56. **Wang X, Zuckerman B, Pearson C, Kaufman G, Chen C, Wang G, Niu T, Wise PH, Bauchner H, Xu X.** Maternal cigarette smoking, metabolic gene polymorphism, and infant birth weight. *JAMA* 287: 195–202, 2002.
57. **Warren BA.** The vascular morphology of tumors. In: *Tumor Blood Circulation: Angiogenesis, Vascular Morphology and Blood Flow of Experimental and Human Tumors*, edited by Peterson HI. Boca Raton, FL: CRC, 1979, p. 1–48.
58. **Whiteley KJ, Pfarrer CD, Adamson SL.** Vascular corrosion casting of the uteroplacental and fetoplacental vasculature in mice. *Methods Mol Med* 121: 371–392, 2006.
59. **Yang J, Yu LX, Rennie MY, Sled JG, Henkelman RM.** Comparative structural and hemodynamic analysis of vascular trees. *Am J Physiol Heart Circ Physiol* 298: H1249–H1259, 2010.